J. Appl. Math. & Informatics Vol. **41***(2023), No. 3, pp. 603 - 613*
https://doi.org/10.14317/jami.2023.603

MEDICAL IMAGE ANALYSIS USING HIGH ANGULAR RESOLUTION DIFFUSION IMAGING OF SIXTH ORDER TENSOR

K.S. DEEPAK AND S.T. AVEESH*

Abstract. In this paper, the concept of geodesic centered tractography is explored for diffusion tensor imaging (DTI). In DTI, where geodesics has been tracked and the inverse of the fourth-order diffusion tensor is inured to determine the diversity. Specifically, we investigated geodesic tractography technique for High Angular Resolution Diffusion Imaging (HARDI). Riemannian geometry can be extended to a direction-dependent metric using Finsler geometry. Euler Lagrange geodesic calculations have been derived by Finsler geometry, which is expressed as HARDI in sixth order tensor.

AMS Mathematics Subject Classification : 53B40, 53C60.
Key words and phrases : Finsler metric, image processing, geodesic equation, diffusion tensor imaging, high angular resolution diffusion imaging.

1. Introduction

Medical images considered in this work are Diffusion Tensor Imaging (DTI) and High Angular Resolution Diffusion Imaging (HARDI) of brain tissue [1,2]. DTI is a non-invasive, magnetic resonance imaging method which evaluates distribution of fluid molecules. A DTI method of magnetic resonance imaging (MRI) evaluates the directional anisotropy of local fluid distribution to map out the formation of nerve tissue in a completely insane way. However, in the areas of complex fiber formation, DTI has some limitations. i.e, in crossing strands do not adequately reflect the distribution area process due to incorrect speculation about the lower distribution area. To overcome these constraints, HARDI [6,8,10] has been introduced, which can better convey the distribution area process.

HARDI image consists of three-dimensional voxels, which are similar to two-dimensional images that combine the same pixels. In a two-dimensional digital

Received August 23, 2022. Revised November 9, 2022. Accepted December 17, 2022.
*Corresponding author.

image, each pixel contains information about the colour and light, where as in the HARDI, each voxels image contains information about the water variation profile [11,12]. The ventricles filled with cerebrospinal fluid functions as storage and support to the brain, during which the defective profiles look like circles as water molecules disperse freely on all sides and it's because in the optic nerve, there are large numbers of nerve connections. In visual cortex, the distribution profiles look like long ellipses, because the molecules are forced to disperse near the nerve bundle, which gives the behavioural collection of water molecules [2,3].

Diffusion orientation distribution function (ODF) [1,2,3,4,5,7] is a very important feature for capturing the angular content of the propagator. A spherical ODF, depicted as a sphere on a unit sphere, represents the diffusion propagator's radial integral in spherical coordinates, and has many variants that are crucial to a number of tractography techniques. The diffusion tensor is an example of a fundamental spherical function that cannot be described by an ellipsoid, but the ODF is a sphere-distributed discrete function. As a result, it can be displayed as a sphere with a colour map, or as a sphere mesh where each vertex has been scaled according to the value of the ODF. These glyphs serve like frequently used visual representations of the ODF and any diffusion signal on the sphere, as well as angular functions.

Neda Sepasian [1,3,7,9] introduces a geodesic equation for HARDI using tractography. Geodesics have been traced using the converse of the second-order diffusion tensor in DTI in order to outline manifold. In order to resolve the complicated fiber populations within a voxel, HARDI models were developed, in which fourth order tensors represent the fiber populations well. Moreover, Finsler geometry is used to produce Euler-Lagrange geodesic equations to assess the other geodesic tractography algorithms, generating the multi-valued numerical model of the geodesic calculations.

In this paper, HRDI will be evaluated using the sixth order tensor of the Riemann-Finsler Geodesic Tractography. In this model, the diffusion profile in the voxel is described by a mode of action in the unit sphere. By using inversion theory [1,2,5], the components of the higher order tensor are reduced from 729 to 28. This numerical model provides the conversion of the spherical harmonic presentation of the ODF into a higher order tensor (HOT) delineation and additional higher order tensor coefficients.

2. Geodesic Equation

Geodesic curve of Finsler metric, which reduces the distance between end-points. Here deliberate a bounded curve C as the variable, x = ξ(t), a$\leq t \leq b$, where t represents the arc-length. The curve C is specified as,

$$J(\xi) = \int_a^b F(\xi(t), \xi(\dot{t}))dt \tag{1}$$

Where $\dot{\xi(t)} = \frac{d(\xi(t))}{dt}$. To minimize the length function, it has been outlined that the required condition (1) must be Euler-Lagrange equations. [11]

$$\frac{d}{dt}\left(\frac{\partial F}{\partial y^\alpha}\right) - \frac{\partial F}{\partial x^\alpha} = 0 \tag{2}$$

Where $y^\alpha = \dot{x^\alpha}$. The geodesic equations will be derived from the Equation (2). Using the chain rule gives as,

$$\frac{d}{dt}\left(\frac{\partial F^2}{\partial y^\alpha}\right) - \frac{\partial F^2}{\partial x^\alpha} = \frac{1}{F}\frac{dF}{dt}\frac{\partial F^2}{\partial y^\alpha} \tag{3}$$

Using that $\frac{dF}{dt} = 0$ (arc length parameterization), the above equations implies to

$$\frac{d}{dt}\left(\frac{\partial F^2}{\partial y^\alpha}\right) - \frac{\partial F^2}{\partial x^\alpha} = 0 \tag{4}$$

Applying the chain rule again and substituting of $g_{\alpha\beta}$=$\frac{1}{2}\frac{\partial^2 F^2}{\partial y^\alpha \partial y^\beta}$yields

$$2g_{\alpha\beta}\ddot{x}^\beta + \frac{\partial^2 F^2}{\partial y^\alpha \partial x^\beta} y^\beta - \frac{\partial F^2}{\partial x^\alpha} = 0 \tag{5}$$

Multiplying Eq. (5) with the inverse $g^{\gamma\alpha}$ gives

$$\ddot{x}^\alpha + 2G^\alpha(x, \dot{x}) = 0 \tag{6}$$

Where G^α are the geodesic coefficients defined by

$$G^\alpha(x, y) = \frac{1}{4} g^{\alpha\beta}(x, y)\left(\frac{\partial^2 F^2(x, y)}{\partial y^\beta \partial x^\gamma} y^\gamma - \frac{\partial^2 F^2(x, y)}{\partial x^\beta}\right) \tag{7}$$

It is often useful to write the geodesic from the point of view of computational, for eq (6), as substitute. To serve this here made it to be revealed the Christoffel symbols of second kind given as

$$\gamma^\alpha_{\beta\gamma}(x, y) = \frac{1}{2} g^{\alpha\beta}(x, y)\left(\frac{\partial g_{\beta k}}{\partial x^\gamma} + \frac{\partial g_{\gamma k}}{\partial x^\beta} - \frac{\partial g_{\beta\gamma}}{\partial x^k}\right) \tag{8}$$

In contrast to the Riemannian case, both space and direction are functions $\gamma^\alpha_{\beta\gamma}$. To reform the geodesic equations, we have to rewrite G^α in concern to the formal Christoffel symbols [4] which has been stated by the following result:

Proposition 1. Geodesic coefficients G^α are defined in equation (7), and their Christoffel symbols $\gamma^\alpha_{\beta\gamma}$ are defined in equation (8) as follows:

$$2G^\alpha = \gamma^\alpha_{\beta\gamma} y^\beta y^\gamma. \tag{9}$$

As a result, derivatives of F are interchanged by derivatives of $g_{\alpha\beta}$ we prove prior to equation (9) we have to have two lemmas. The first is of Cartan's connection $C_{\alpha\beta\gamma}$(x,y) is defined as:

$$C_{\alpha\beta\gamma} = \frac{1}{4}\frac{\partial^3 F^2(x, y)}{\partial y^\alpha y^\beta y^\gamma}.$$

Lemma 1. *The Cartan tensor* $C_{\alpha\beta\gamma}(x,\ \mathrm{y})$ *gratifies*

$$C_{\alpha\beta\gamma}\,(x,\ \mathrm{y})\,y^{\gamma}=0. \tag{10}$$

Proof. The Riemann-Finsler metric $g_{\alpha\beta}(x,\ \mathrm{y})$ receives the below mentioning homogeneous property from the fixed property $\mathrm{F}(x,\ \lambda\ \mathrm{y}) = \lambda\mathrm{F}(\mathrm{x},\ \mathrm{y})$ for all $\lambda>0$:

$$g_{\alpha\beta}(x,\lambda y) = g_{\alpha\beta}(x,y).$$

Differentiation concerning to λ and while setting $\lambda = 1$ gives

$$\frac{\partial g_{\alpha\beta}(x,y)}{\partial y^{\gamma}}y^{\gamma} = 0.$$

As a result, the Cartan tensor satisfies

$$C_{\alpha\beta\gamma}(\mathrm{x},\ \mathrm{y})y^{\gamma}=\tfrac{1}{2}\tfrac{\partial g_{\alpha\beta}(x,y)}{\partial y^{\gamma}}y^{\gamma}=0.$$

Lemma 2. In Riemann-Finsler metric tensor, equations hold

$$g_{\alpha\beta}y^{\alpha}y^{\beta} = F^2 \tag{11}$$

$$\frac{\partial}{\partial y^{\gamma}}\left(g_{\alpha\beta}y^{\alpha}y^{\beta}\right) = 2g_{\gamma\alpha}y^{\alpha} \tag{12}$$

Proof: The following equations can be derived from the homogeneity of F,

$$\frac{\partial F}{\partial y^{\alpha}}y^{\alpha} = F, \quad \frac{\partial^3 F}{\partial y^{\alpha}\partial y^{\beta}}y^{\beta} = 0.$$

First the relation (11) is proved by using definition $g_{\alpha\beta}=\tfrac{1}{2}\tfrac{\partial^2 F^2}{\partial y^{\alpha}\partial y^{\beta}}$ it's seen that

$$\begin{aligned} g_{\alpha\beta}y^{\alpha}y^{\beta} &= \frac{1}{2}\frac{\partial}{\partial y^{\alpha}}\left(\frac{\partial F^2}{\partial y^{\beta}}\right)y^{\alpha}y^{\beta} \\ &= \frac{\partial}{\partial y^{\alpha}}\left(F\frac{\partial F}{\partial y^{\beta}}\right)y^{\alpha}y^{\beta} \\ &= \left(\frac{\partial F}{\partial y^{\alpha}}\frac{\partial F}{\partial y^{\beta}} + F\frac{\partial^2 F^2}{\partial y^{\alpha}\partial x^{\beta}}\right)y^{\alpha}y^{\beta} \\ &= \frac{\partial F}{\partial y^{\gamma}}\frac{\partial F}{\partial y^{\beta}}y^{\alpha}y^{\beta} = F^2. \end{aligned}$$

Using the above equation (11), we show equation (12) by having

$$\begin{aligned} \frac{\partial}{\partial y^{\gamma}}\left(g_{\alpha\beta}y^{\alpha}y^{\beta}\right) &= \frac{\partial g_{\alpha\beta}}{\partial y^{\gamma}}y^{\alpha}y^{\beta} + g_{\alpha\beta}\delta_{\alpha\gamma}y^{\beta} + g_{\alpha\beta}y^{\alpha}\delta_{\beta\gamma} \\ &= 2C_{\alpha\beta\gamma}y^{\alpha}y^{\beta} + 2g_{\gamma\beta}y^{\beta}. \end{aligned}$$

Proof of Proposition 1 As a result of the above lemmas, the next derivation gives us to express G^{α} in relations of Christolfel signs, i.e.,

$$\begin{aligned} 2G^{\alpha} &= \frac{1}{2}g^{\alpha\beta}\left(\frac{\partial}{\partial x^{\gamma}}\frac{\partial F^2}{\partial y^{\beta}}y^{\gamma} - \frac{\partial F^2}{\partial x^{\beta}}\right) \\ &= \frac{1}{2}g^{\alpha\beta}\left(\frac{\partial}{\partial x^{\gamma}}\frac{\partial}{\partial y^{\beta}}\left(g_{\lambda\mu}y^{\lambda}y^{\mu}y^{\gamma}\right) - \frac{\partial g_{\lambda\mu y^{\lambda}y^{\mu}}}{\partial x^{\beta}}\right), \end{aligned}$$

where expression (11) is substituted for F^2. Next combining this relation with (12), it's obtained

$$2G^{\alpha} = \frac{1}{2}g^{\alpha\beta}\left(\frac{\partial}{\partial x^{\gamma}}\left(2g_{\beta\mu}y^{\lambda}\right)y^{\gamma} - \frac{\partial g_{\lambda\mu}}{\partial x^{\beta}}y^{\lambda}y^{\mu}\right)$$
$$= \frac{1}{2}g^{\alpha\beta}\left(\frac{\partial g_{\lambda\beta}}{\partial x^{\mu}} + \frac{\partial g_{\mu\beta}}{\partial x^{\lambda}} - \frac{\partial g_{\lambda\mu}}{\partial x^{\beta}}\right)y^{\lambda}y^{\mu}.$$

Hence the proof of equation (9). Substituting equation (9) in (10) gives

$$\ddot{x} + \Gamma^{\alpha}_{\beta\gamma}\dot{x}^{\beta}\dot{x}^{\gamma} = 0. \tag{13}$$

This is another form of the geodesic equation.

3. Numerical Model

In the HARDI model, the sixth-order tensor illustration has been considered of the Orientation Distribution Function (ODF) [1, 5, 6, 7]. Based on the transformation of the basis, the ODF's spherical harmonics representation can be changed into a HOT representation. To calculate Finsler metrics, the circular inversion of the ODF on each voxel must be calculated. To do this, Eq (3) on the unit sphere for m> 28 is applied, which determines the system $\boldsymbol{Y}\widetilde{\mathrm{d}}=\mathbf{b}$. where $\widetilde{\mathrm{d}}$ consists the coefficients; See the Table 1.

Table 1: HOT coefficients

Tensor element	HOT Coefficient	Tensor element	HOT Coefficient	Tensor element	HOT Coefficient	Tensor element	HOT Coefficient
1	D_{111111}	8	D_{333331}	15	D_{333322}	22	D_{111223}
2	D_{222222}	9	D_{333332}	16	D_{111222}	23	D_{111332}
3	D_{333333}	10	D_{111122}	17	D_{111333}	24	D_{222113}
4	D_{111112}	11	D_{111133}	18	D_{222333}	25	D_{222331}
5	D_{11113}	12	D_{222211}	19	D_{111123}	26	D_{333112}
6	D_{222221}	13	D_{222233}	20	D_{222213}	27	D_{333221}
7	D_{222223}	14	D_{333311}	21	D_{333312}	28	D_{112233}

The icosahedron tessellation on the unit sphere has been applied to ensure uniform pattern orientation y on the sphere. It's limited to the formalise ODF, so $\overline{\mathrm{P}}_6(\mathrm{x,y}) = 1$. To find the result to this arrangement, least squares approximation method has been applied. The rewrite of the equation in general is as $\boldsymbol{Y}^T\boldsymbol{Y}\widetilde{\mathrm{d}} = \mathrm{Y}^T\mathbf{b}$.

$$\boldsymbol{Y} = \begin{pmatrix} y_1^1 y_1^1 y_1^1 y_1^1 & \cdots & y_1^3 y_1^3 y_1^3 y_1^3 \\ y_2^1 y_2^1 y_2^1 y_2^1 & \cdots & \cdots \\ \vdots & \vdots & \vdots \\ y_m^1 y_m^1 y_m^1 y_m^1 & \cdots & y_m^3 y_m^3 y_m^3 y_m^3 \end{pmatrix}, \quad \mathbf{b} = \begin{pmatrix} P_6(\mathrm{x,y_1})^{-1} \\ \vdots \\ P_6(\mathrm{x,y_m})^{-1} \end{pmatrix}. \tag{14}$$

The lower indices in y denote the gradient direction and m is the numerical figure of gradient directions to be sampled from ODF profile; m is set as 729 components in the computations. The solution $\widetilde{\mathrm{d}}$ is calculated by using Cholesky factorization method, which reduces to 28 co-efficient for the inverted ODF profile. The new profile can be fitted over the sphere using the new co-efficient $\widetilde{\mathrm{d}}$ **;** see Fig 1

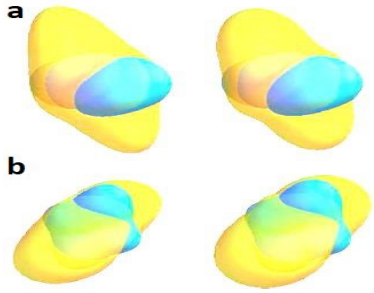

Fig. 1 ODF and its inverse using lest-squares fit (Left) and analytic inversion (Right). (a) ODF and its inverse for a single fiber image (b) ODF its inverse for a crossing fiber image.

Let it be introduced $u^{\gamma}(t) := x^{\gamma}(t)$ for $\gamma = 1, 2, 3$, then it can be rewritten in system (13) as,

$$\dot{x}^{\alpha} = u^{\alpha},$$
$$u^{\alpha} = \Gamma^{\alpha}_{\beta\gamma}\mathrm{u}^{\beta}\mathrm{u}^{\gamma}, \tag{15}$$

with the $\Gamma^{\alpha}_{\beta\gamma}$defined in (15). Sepasian et al. [11] proposed a similar technique to resolve the system of equations (22). Consider $(\mathrm{x}^1(0), \mathrm{x}^2(0), \mathrm{x}^3(0)$ as a point in the area and $(\mathrm{u}^1(0), \mathrm{u}^2(0), \mathrm{u}^3(0))$ as the preliminary path. The Runge-Kutta method of ODE, with the fourth order explicit method, was used to calculate the solutions to (15) using the given initial point and multiple directions and to produce a set of geodesics linking the specified point to a set of boundary points.

It is divided regularly through grid extent h and grid points $\mathrm{x}_{ijk} = (\mathrm{x}^1_{\mathrm{i}}, \mathrm{x}^2_{\mathrm{j}}, \mathrm{x}^3_{\mathrm{k}})$ $= \boldsymbol{h(i,j,k)}$ for $\boldsymbol{i} = 0,2,3,\ldots,N$ - 1, where N is the number of grid points in each spatial direction. For easiness, the number of grid points equal in all directions have been taken. For each grid point, there assigned 28 coefficients of inverted Higher Order Tensor $\tilde{D}$.

Based on a standard second order vital difference scheme, we have approximated $\mathrm{g}_{\boldsymbol{\alpha\beta}}(\mathrm{x,y})$ in each grid point, for example,

$$\frac{\partial \mathrm{g}_{\alpha\beta}}{\partial \mathrm{x}^1}\left(x^1_i\ ,\ x^2_j\ ,\ x^3_k,\ \mathrm{y}\right) \approx \frac{1}{2h}\left(\mathrm{g}_{\alpha\beta}\left(x^1_{i+1}\ x^2_j\ ,\ x^3_k,\ y\right) - \mathrm{g}_{\alpha\beta}\left(x^1_{i-1}\ x^2_j\ ,\ x^3_k,\ y\right)\right). \tag{16}$$

Second order variances are calculated when grid points are located on a boundary,
$\frac{\partial g_{\alpha\beta}}{\partial x^1}\left(x_i^1\ ,\ x_j^2\ ,\ x_k^3,\ y\right)\approx$

$$\frac{1}{2h}\left(-3g_{\alpha\beta}\left(x_0^1 x_j^2\ ,\ x_k^3,\ y\right)+4g_{\alpha\beta}\left(x_0^1 x_j^2\ ,\ x_k^3,\ y\right)-g_{\alpha\beta}\left(x_0^1 x_j^2\ ,\ x_k^3,\ y\right)\right). \tag{17}$$

Similarly, derivatives of x^2 and x^3 can also be computed, while keeping in mind that these relationships depend on the argument y. ODE, however, provides solutions that do not necessarily correspond to grid points. So, the value of a metric and its derivatives is not defined, and the trilinear interpolation is used where the value does not available. The initial vectors have been distributed equally on the unit area using the various simple symmetric polyhedral. Consolidation of geodesics extends until the computation reaches the end point of the domain. The initial seed points for the geodesics have been calculated as the starting point will be set and then the fibers can be selected by selecting the areas of interest and filtering all the geodesics passing through the two selected areas. A geodesic is calculated until it meets one of the boundary lines, then a line-plane intersection is performed to pinpoint the fibers that connect the two given areas. The selected fields can be truncated with this after entering a geodesic.

4. Finsler Metric

Higher order tensors would be developed versions of second order tensors. Multiple fiber orientations can be represented with higher order tensors. Simple, the theory has been introduced for sixth order tensors, but can be ignorable extended to higher orders. In the HARDI model, $P_6(x,\ y)$ is a purpose on the unit sphere which represents the diffusion profile. This theory has been accessible in a common form such as $P_6(x,\ y)$, which can be a diffusive profile that results from diverse HARDI modelling strategies so long as the diffusion flux increases along with cumulative standards $P_6(x,\ y)$.
Using specimen data on a unit sphere, the coefficients of the sixth order tensor have been fixed to D = D(x) to the function $P_6(x,\ y)$.[6], i.e.,

$$P_6(x,\ y) = D_{pqrstu}(x) y^p y^q y^r y^s y^t y^u \tag{18}$$

with $(p, q, r, s, t, u) = 1, 2, 3, 4, 5, 6$, i=1, 2, 3, 4, 5, 6, x contains the spatial coordinate where $y=y^p y^q y^r y^s y^t y^u=(\sin\theta\cos\emptyset,\ \sin\theta\sin\emptyset,\ \cos\theta)$ is the directional vector with $\emptyset \in [0,\ 2\pi)$ and $\theta \in [0.\pi\ ]$. Here, the coefficients $D_{pqrstu}(x)$ are the perticles of D. Einstein summation is employed in all formulas, i.e., repeated indexes have been summed up, one for each position in the superscript and subscript. Tensor D satisfies the symmetry property,

$$D_{pqrstu} = D_{\sigma(p)\sigma(q)\sigma(r)\sigma(s)\sigma(t)\sigma(u)}. \tag{19}$$

For any permutation σ, therefore the number of components can be reduced from 729 to 28.

The DTI Riemannian method is a heuristic approach used to find the probability of a fiber extending in the system of y matches to a larger diffusivity denoted in $\mathrm{P}_6(x,y)$, as well as faster diffusion. Thus, the metric must be given the shortest distance in the way where diffusion is greater. This has been attained by using the metric as the converse of the diffusion tensor in DTI. Thus, the diffusion tensor's largest eigen value is the metric's smallest. On the other hand, HARDI allows for the analysis of diffusion profiles that are more complex. This method needs to be prolonged to include Finsler metric for the purpose of position and direction. To invert the HOT, a suitable framework needs to be developed. A proper inversion requires certain properties to be preserved, for the normal value of the function in the angle between two directions [3]. In Figure 2, Astola explains the spherical inversion of a point on a surface M by coordinate's x_M [2] .A point M' is the inverse of a given point M with respect to a sphere with radius $r = a$. This means that $|\mathrm{x}_M|\times|\mathrm{x}_{M'}|=a^2$ in spherical coordinates, where $\mathrm{x} = re_r$ is the position vector and e_r is the radial unit vector. There are two points M and M' on the same ray through O. The figure 2 shows the inversion maps from points**,**

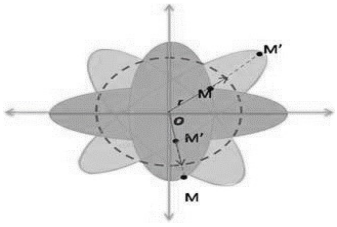

Fig. 2 A two-dimensional illustration of spherical inversion. M' is M' in terms of a circle.

within the sphere to points outside it and vice versa. As an example, when M is outside the given sphere, $|\mathrm{x}_M|>$ n gives,

$$|\boldsymbol{x}_{\boldsymbol{M'}}|=\frac{\boldsymbol{a^2}}{|\boldsymbol{x}_{\boldsymbol{M}}|} < a.$$

In similitude with the spherical inversion, $\widetilde{P_6}(\mathrm{x},\ \mathrm{y})$ has been defined that is the inverse of $\mathrm{P}_6(\mathrm{x},\mathrm{y})$, is as follows,

$$\widetilde{\mathrm{P}_6}(x,\ \ y) = \frac{\overline{P_6}(\mathrm{x},\ \ \mathrm{y})}{P_6(\mathrm{x},\ \ \mathrm{y})} = D_{pqrstu}(x)y^p y^q y^r y^s y^t y^u, \tag{20}$$

where D is HOT that fits $\widetilde{\boldsymbol{P_6}}(\mathrm{x},\mathrm{y})$ and $\overline{\boldsymbol{P_6}}(\boldsymbol{x},\ \boldsymbol{y})$is the normal of HOT over the unit sphere, i.e.,

$$\overline{\mathrm{P}_6}(x,\ y)=\int_{|y|=1} \mathrm{P}_6(x,\ \ y)\, dy.$$

Astola, present the next Finsler norm for the sixth order tensors

$$F(x,y) = \left(\widetilde{\mathrm{P}}_6(x,y)\right)^{\frac{1}{6}}. \tag{21}$$

The Finsler metric is considered by the bilinear form $F=F(x,y)$ is as given

$$g_{\alpha\beta}=\frac{1}{2}\frac{\partial^2 F^2}{\partial y^\alpha \partial y^\beta}\ , \tag{22}$$

where α and β are used to index the components of tensor g.

As explained below, the Riemannian metric is a special case of the Finsler metric. If $F^2\ (x.y) = g_{\alpha\beta}\ (x) y^\alpha y^\beta$ i.e $g_{\alpha\beta}$ only depends on x, then,

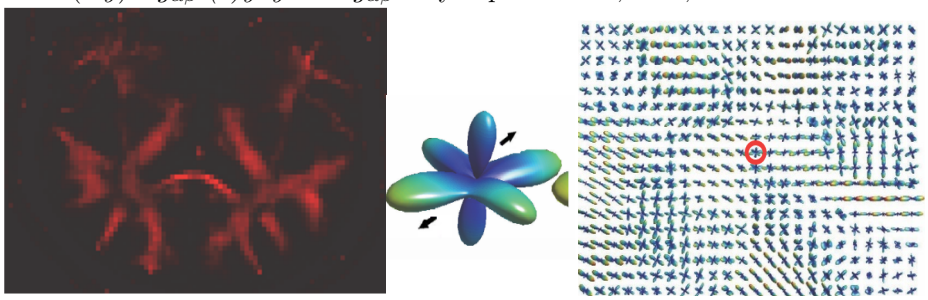

(a) **(b)** **(c)**

Figure 3 (a) Explanation of the directional dependence of tensors $g_{\alpha\beta}$ (x, y). (b) and (c) The $\widetilde{P_6}$(x, y) , appearing as a surface in all images.

In each image, the arrows indicate specific directions y, and the ellipsoids represent the tensors x, y) calculated from (x, y), by fixing the direction y.

$$g_{\alpha\beta}(x,\ y) = \frac{1}{2}\frac{\partial^2}{\partial y^\alpha \partial y^\beta}(g_{\alpha\beta}(x) y^\alpha y^\beta) = g_{\alpha\beta}(x). \tag{23}$$

This metric is recognized as Riemannian metric. By difference, Finsler metric is not lone influenced by x, but also by y. Astola has analysed the required conditions of differentiability, homogeneity, and strong convexity for (21) found that the strong convexity criterion only applies if fourth order tensor $D_{pqrstu} y^p y^q y^r y^s$ is positive definite for every y.

Substituting (21) for the bilinear form (22), the Finsler metric tensor reads could be made visible as,

$$\begin{aligned} g_{\alpha\beta}(x,\ y)\ &= \frac{1}{2}\frac{\partial^2 F^2}{\partial y^\alpha \partial y^\beta} \\ &= -4\tilde{P}_6(x,y)^{\frac{-5}{3}}(D\ _{\alpha pqrst} y^p y^q y^r y^s y^t)(D\ _{\beta pqrst} y^p y^q y^r y^s y^t) \\ &\quad + 5\tilde{P}_6(x,y)^{\frac{-2}{3}}(D\ _{\alpha pqrst} y^p y^q y^r) \end{aligned} \tag{24}$$

In this case, the corresponding local metric can be obtained at each position and y. Figure 3 depicts the Finsler metric's directional dependence on a $\widetilde{\boldsymbol{P_6}}(\boldsymbol{x}, \boldsymbol{y})$ profile. Three tensors $\boldsymbol{g_{\alpha\beta}}(\boldsymbol{x}, \boldsymbol{y})$ can be derived from the same position, i.e., x, by altering y. The metric tensors are essential to calculate the geodesics in Finsler geometry.

5. Conclusion

An algorithm for tractography of HARDI data has been proposed. It is based on the calculation of geodesics impression in the Finsler metric, which is an extension of the Riemannian metric. The Finsler metric has been defined as the function of position, and for its direction, HARDI information has been extracted from each voxel. This includes the diffusion profile within a voxel which is described by the function in the unit sphere. By applying inversion theory, reduce the components of the higher order tensor from 729 to 28. The numerical model provides the transformation of the spherical harmonic image of the ODF into a higher order tensor image and higher order tensor coefficients. A heuristic choice has been made for the mapping of HARDI data to the Finsler metric. The theory that suggests a possible method of extracting crossing fiber has been presented.

Conflicts of interest : The authors declare no conflict of interest.

Data availability : No data were used to support this paper.

Acknowledgments : The authors wish to express their sincere thanks to the reviewer for the valuable suggestions.

References

1. N. Sepasian, H.M. Jan, T. Boonkkamp, Luc M.J. Florack, Bart M. Ter Haar Romeny and Anna Vilanova, *Riemann-FinslerMulti-valued Geodesic Tractography for HARDI. Visualization and Processing of Tensors and Higher Order Descriptors for Multi-Valued Data*, Springer, Berlin, Heidelberg, 2014, 209-225.
2. L. Astola, *Multi-Scale Riemann-Finsler Geometry Applications to Diffusion Tensor Imaging and High Angular Resolution Diffusion Imaging*, Ph.D. Thesis , Eindhoven University of Technology, the Netherlands, 2010.
3. I. Aganj, C. Lenglet, and G. Sapiro, *ODF reconstruction in q-ball imaging with solid angle consideration*, Proceedings of the Sixth IEEE International Symposium on Biomedical Imaging **47** (2009), 392–397.
4. L. Astola and L. Florack, *Finsler geometry on higher order tensor fields and applications to high angular resolution diffusion imaging*, International Journal of Computer Vision **42** (2011), 325–336.
5. D.E. Blarr, *Inversion Theory and Conformal Mapping*, American Mathematical Society, Proceedings, 2000.
6. S. Chern, Z. Shen, *Lectures on Finsler geometry*, Nankai Tracts Math. **25** (2003), 63-76,139-147,203-215.
7. M. Descoteaux, *High angular resolution diffusion MRI: from local estimation to segmentation and tractography*, Ph.D. Thesis, Universite de Nice, Sophia Antipolis, 2005.
8. M. Descoteaux, E. Angelino, S. Fitzgibbons, R. DericheR, *Regularized, fast and robust analytical q-ballimaging*, Magn. Reson. Med. **58** (2007), 498-508.

9. A. Tristan Vega, C.F. Westin, S. Aja-Farnandez, *Estimation of fiber orientation probability density functions in high angular resolution diffusion imaging*, Neuro Image **47** (2009), 638-650.
10. P.J. Basser, J. Mattiello, R. Turner, D. LeBihan, *Diffusion tensor echo-planar imaging of human brain*, Proceedings of the SMRM **56** (1993), 584-592.
11. P.J. Basser, J. Mattiello, D. Lebihan, *Estimation of the effective self-diffusion tensor from the NMR spin echo*, Journal of Magnetic Resonance Series B **103** (1994), 247-254.
12. P.J. Basser, J. Mattiello, D. Lebihan, *MR diffusion tensor spectroscopy and imaging*, Biophysical Journal **66** (1994), 259-267.

K.S. Deepak received M.Sc. from Kuvempu University and doing Ph.D. at Visweswrayya Technological University. Currently he is working as Assisent Professor, Department of Mathematics, Alva's College ,Moodubidire. His research interests include Diffrential geometry, Finsler Geometry and its Applications in biological computation.

Department of Mathematics, Alva's College, Moodubidire, Dakshina kannada, Karnatak Pin-574227, India.
e-mail: deepakpatel2124@gmail.com

S.T. Aveesh received M.Sc. and Ph.D. from Kuvempu University. Currently he is working as Professor, Department of Mathematics, PES Institute of Technology and Management Shivamogga. His research interests include Diffrential geometry, Finsler Geometry and its Applications in biological computation.

Department of Mathematics, PES Institute of Technology and Management, Sagar Road, Shivamogga, Karnataka, INDIA -577204.
e-mail: aveeshst@gmail.com